Computer Modeling in Engineering & Sciences

Tech Science Press

DOI: 10.32604/cmes.2023.025993

ARTICLE

Improved Prediction of Slope Stability under Static and Dynamic Conditions Using Tree-Based Models

Feezan Ahmad[1], Xiaowei Tang[1], Jilei Hu[2,*], Mahmood Ahmad[3,4] and Behrouz Gordan[5]

[1]State Key Laboratory of Coastal and Offshore Engineering, Dalian University of Technology, Dalian, 116024, China

[2]Key Laboratory of Geological Hazards on Three Gorges Reservoir Area, Ministry of Education, China Three Gorges University, Yichang, 443002, China

[3]Department of Civil Engineering, Faculty of Engineering, International Islamic University Malaysia, Jalan Gombak, Selangor, 50728, Malaysia

[4]Department of Civil Engineering, University of Engineering and Technology Peshawar (Bannu Campus), Bannu, 28100, Pakistan

[5]Faculty of Civil Engineering, Islamic Azad University, Varamin Pishva Branch, Tehran, 15914, Iran

*Corresponding Author: Jilei Hu. Email: hujl@ctgu.edu.cn

Received: 09 August 2022 Accepted: 23 December 2022

ABSTRACT

Slope stability prediction plays a significant role in landslide disaster prevention and mitigation. This paper's reduced error pruning (REP) tree and random tree (RT) models are developed for slope stability evaluation and meeting the high precision and rapidity requirements in slope engineering. The data set of this study includes five parameters, namely slope height, slope angle, cohesion, internal friction angle, and peak ground acceleration. The available data is split into two categories: training (75%) and test (25%) sets. The output of the RT and REP tree models is evaluated using performance measures including accuracy (*Acc*), Matthews correlation coefficient (*Mcc*), precision (*Prec*), recall (*Rec*), and *F-score*. The applications of the aforementioned methods for predicting slope stability are compared to one another and recently established soft computing models in the literature. The analysis of the *Acc* together with *Mcc*, and *F-score* for the slope stability in the test set demonstrates that the RT achieved a better prediction performance with ($Acc = 97.1429\%$, $Mcc = 0.935$, *F-score* for stable class $= 0.979$ and for unstable case *F-score* $= 0.935$) succeeded by the REP tree model with ($Acc = 95.4286\%$, $Mcc = 0.896$, *F-score* stable class $= 0.967$ and for unstable class *F-score* $= 0.923$) for the slope stability dataset The analysis of performance measures for the slope stability dataset reveals that the RT model attains comparatively better and reliable results and thus should be encouraged in further research.

KEYWORDS

Slope stability; seismic excitation; static condition; random tree; reduced error pruning tree

1 Introduction

In geotechnical engineering, slope stability analysis and prediction are critical. Along with earthquakes and volcanoes, slope instability has become one of the world's three great geological disasters. To decrease or prevent landslide damage, slope stability analysis and stabilization are

required. Nevertheless, accurate slope stability prediction is difficult due to the complexity of slope structures and the difficulty in identifying the relevant input data linked to significant geotechnical parameters [1–3].

Several approaches have been proposed to analyze or predict slope stability, among which are Limit Equilibrium Methods (LEMs) [4,5] and numerical methods (e.g., Finite-element Method (FEM)) [6–8] are the most widely employed methods [9,10]. Empirical equations [11,12] and limit analysis approaches based on lower and upper bound theorems [13] are other methods. All of the methods discussed above, however, have some drawbacks. Limit equilibrium methods, for example, cannot reflect the slip surfaces' actual stress conditions [14], and as a result of simplifying assumptions, their accuracy is compromised [1]. The numerical methods are time-consuming, and their accuracy is strongly reliant on correct geotechnical and physical parameter estimation.

For the last few years, a recently developed approach based on data mining techniques has been increasingly used to solve real-world problems, particularly in the field of civil engineering [15–35]. Several practical problems have already been successfully solved with machine learning algorithms, paving the way for new prospects in civil engineering. Furthermore, a variety of machine learning algorithms, for example, Artificial Neural Networks (ANNs) and Support Vector Machine (SVM) have been developed for addressing technical issues, such as predicting slope stability [10,36]. Table 1 summarizes previous studies on slope stability prediction using soft computing techniques. ANN and SVM are the most widely used soft computing methods for predicting slope stability because they do not require prior knowledge of a specific model form and have flexible nonlinear modeling capabilities [37]. They also outperform traditional analytical and regression methods when it comes to predicting slope stability [38,39].

Table 1: Previous research on slope stability prediction using soft computing approaches

Model	Input	Data size	Reference
FFNN	γ, c, ϕ, β, H, ru	82 cases	Feng [40]
BPNN	γ, c, ϕ, β, H, ru	32 cases	Lu et al. [41]
ANN and ANFIS	γ, c, ϕ, β, H	59 cases	Li [42]
CNN	γ, c, ϕ, β, H, ru	64 cases	Huang et al. [43]
BPNN	γ, c, ϕ, β, H, ru	46 cases	Sakellariou et al. [1]
BPNN	γ, c, ϕ, β, H	27 cases	Wang et al. [44]
SVM	γ, c, ϕ, β, H, ru	46 cases	Samui [45]
SVM	γ, c, ϕ	10 cases	Zhao [46]
ANN	X, Y, S_r, c, ϕ, β, a_h, a_v	36 cases	Choobbasti et al. [47]
ANN	γ, c, ϕ, β, H, r_u	46 cases	Das et al. [48]
ANN	γ, c, ϕ, β, H	675 modeled cases	Erzin et al. [38]
ELM	γ, c, ϕ, β, H, r_u	97 cases	Liu et al. [9]
PSO–ANN	c, ϕ, β, H, PGA	699 modeled cases	Gordan et al. [36]
LS-SVC	γ, c, ϕ, β, H, r_u	168 cases	Hoang et al. [49]
FNs, MARS, MGGP	γ, c, ϕ, β, H, r_u	103 cases	Suman et al. [3]
FEM-ANN	c, ϕ, β, pp	100 modeled cases	Verma et al. [50]
PSO–ANN	γ, c, ϕ, β, H, r_u	83 cases	Rukhaiyar et al. [51]
PSO–LSSVM	γ, c, ϕ, β, H, r_u	46 cases	Xue [10]

(Continued)

Table 1 (continued)

Model	Input	Data size	Reference
NBC	γ, c, ϕ, β, H, r_u	82 cases	Feng et al. [52]
GBM	γ, c, ϕ, β, H, r_u	221 cases	Zhou et al. [53]
TAN	γ, c, ϕ, β, H, r_u	87 cases	Ahmad et al. [54]
DT, RF, AdaBoost	c, ϕ, β, H, PGA	700 modeled cases	Asteris et al. [55]

Note: γ Unit weight, c Cohesion, ϕ Internal friction angle, β Slope angle, H Slope height, r_u Pore pressure ratio, pp Pore pressure, X X coordinate, Y Y coordinate, S_r Degree of saturation, a_h Horizontal coefficient of earthquake, a_v Vertical coefficient of earthquake, PGA Peak ground acceleration, FFNN Feed forward neural network, BPNN Back-propagation neural network, ANN Artificial Neural Networks, ANFIS Adaptive neuro-fuzzy inference system, CNN Chaotic Neural Network, SVM Support vector machine, ELM Extreme learning machine, PSO Particle swarm optimization, LS-SVC Least squares support vector classification, FNs functional networks, MARS Multivariate adaptive regression splines, MGGP Multigene genetic programming, LSSVM least squares support vector machine, NBC Naive-Bayes classifier, GBM Gradient boosting machine, TAN Tree augmented Naive-Bayes classifier, DT Decision tree, RF Random forest, AdaBoost adaptive boosting.

As shown in Table 1, various researches classified slope FoS under static conditions using essential factors such as slope height (H), cohesion (c), internal friction angle (ϕ), slope angle (β), and unit weight (γ). These studies presented novel ideas and methods for predicting slope stability. On the other hand, this field is still being researched. According to a critical review of the existing literature, despite the successful implementation of the reduced error pruning (REP) tree and random tree (RT) in various domains, e.g., [19,56], their application to predict slope stability in dynamic situations is scarcely explored. In the current study, the horizontal component of peak ground acceleration (PGA) is included in the input parameters.

This study has significance in several ways:

1. Decision tree models are developed for analyze and early detection of slope stability that able to learn the complex relationship between slope stability and its influencing factors with reasonable precision. Furthermore, the proposed models provide easily interpretable tree structures that can be used by geotechnical engineering professionals with the help of spreadsheets to predict the slope stability for future seismic events without going into the complexities of models development using RT and REP trees.
2. The performance of the proposed models is comparatively assessed with two commonly used soft computing models (RF and AdaBoost) published in the literature to validate the performance.
3. One of the major advantages of the presented models is the consideration and addition of dynamic conditions—the horizontal component of peak ground acceleration (PGA) to the database.
4. Data division for training and testing datasets was carried out with due regard for statistical aspects such as dataset range, mean, and standard deviation. The datasets are split to determine the predictive ability and generalization performance of developed models, which will and later helps in evaluating them better.

The following summarizes the rest of the paper: The data catalog is shown in Section 2. Section 3 describes the applied DT techniques and performance measures. The results and discussion are presented in Section 4. Finally, some concluding remarks are given.

2 Data Catalog

In this study, 700 homogenous slope data (see Appendix A) were obtained from [55] and simulated using GeoStudio, which utilizes the LEM approach for the most important FoS parameters. Many homogenous slopes (in terms of material, $\gamma = 18\,kg/m^3$) with varied conditions were modeled to achieve FoS in the study. The slopes were created with heights of 15, 20, 25, and 30 m with slopes of 20°, 25°, 30°, and 35°. In terms of rigid behavior, all of the models were on bedrock. Furthermore, all models were supposed to have a crest width of 8 m. The failure criterion of Mohr-Coulomb was applied in this study's analysis. Internal friction angles of 20°, 25°, 30°, 35°, and 40° were utilized in the tests, with cohesions of 20, 30, 40, and 50 kPa. All models were assumed to have a soil density of $18\,kg/m^3$. According to Kramer [57], peak ground acceleration (PGA) is a measurement of earthquake acceleration on the ground. The PGA amplitudes were determined to be 0.1, 0.2, 0.3, and 0.4 g in this investigation. FoS values were determined for several slope scenarios. As slip surfaces, all of the slope models used thirty slices. This study used a grid and a radius slip surface to achieve FoS values. The computed FoS in the grid and radius technique should be almost in the grid's center. Previous studies (e.g., [55]) show that slope stability under seismic excitation is a function of slope height (H), cohesion (c), internal friction angle (ϕ), slope angle (β), and peak ground acceleration (PGA). Therefore, in the current study, these input variables were used to develop the proposed models. Fig. 1 illustrates a generic limit equilibrium model for the simulated slope. Table 2 shows the statistics for all five input parameters (i.e., c, ϕ, β, H, and PGA) in the database, including their range, mean, standard deviation (Std. Dev), and coefficient of variation (COV). Fig. 2 is a heat map of a correlation matrix that highlights the correlation between parameters. It should be noticed that c, ϕ, and H have the highest variations.

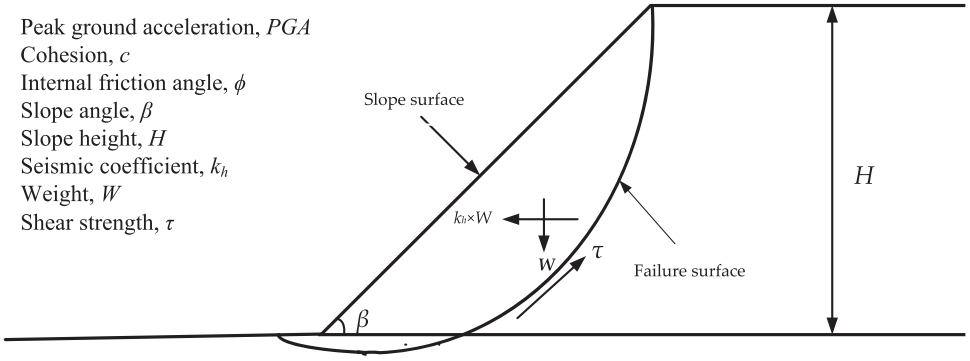

Figure 1: Limit equilibrium model for the stability analysis

Table 2: Input and output parameters for classifying slope stability

Parameter	Unit	Dataset	Range	Mean	Std. Dev	COV
Slope height, H	m	Training	15–30	19.848	4.095	0.206
		Testing	25–30	29.800	0.983	0.033
		Total	15–30	49.648	5.078	0.239
Slope angle, β	°	Training	20–35	25.010	5.024	0.201
		Testing	20–35	25.686	5.476	0.440
		Total	20–35	50.696	10.5	0.641

(Continued)

Table 2 (continued)

Parameter	Unit	Dataset	Range	Mean	Std. Dev	COV
Cohesion, *c*	kPa	Training	20–50	35.143	11.216	0.319
		Testing	20–50	35.771	11.108	0.311
		Total	20–50	70.914	22.324	0.630
Internal friction angle, ϕ	°	Training	20–40	33.981	5.906	0.174
		Testing	20–40	34.371	5.814	0.169
		Total	20–40	68.352	11.72	0.343
Peak ground acceleration, PGA	m/s^2	Training	0–3.924	1.211	1.084	0.895
		Testing	0–3.924	1.087	1.022	0.940
		Total	0–3.924	2.298	2.106	1.835
Factor of safety, *FoS*	-	Training	0.783–2.457	1.196	0.354	0.296
		Testing	0.789–2.391	1.194	0.341	0.286
		Total	0.783–2.457	2.39	0.695	0.582

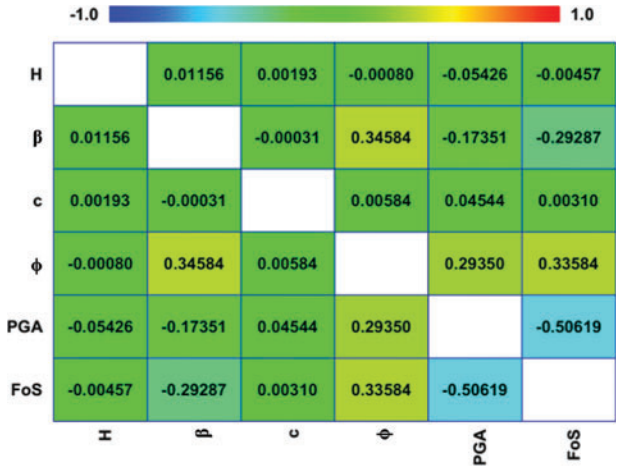

Figure 2: Heat map displaying the correlation matrix between five input variables and one output variable in the dataset

3 Methodology

3.1 Random Tree

Random trees comprise a forest of predictor trees. The random tree is an algorithm halfway between a simple decision tree and a random forest. Random trees were initially proposed by Leo Breiman and Adele Cutler. The algorithm can address both regression and classification tasks [58,59]. The classification mechanisms include the following: The random tree classifier classifies the input vector of characteristics with each tree in the forest and then outputs the class label with the most "votes" [60].

A random tree is one that is randomly created from a set of possible trees, each of which has K random attributes at each node. In this context, "at random" indicates that any tree in the set has an equal chance of being chosen for sampling. Rapidly constructing random trees and integrating them with large sets of random trees typically yields accurate models. In recent years, there has been extensive research on random trees in the field of machine learning, e.g., [58]. The random tree approach is employed in order to achieve the highest level of accuracy in its numerous classifier parameters such as a minimum number of instances and the number of sets utilized for randomly chosen attributes. The decision tree must be basic and compact for improved classification. Otherwise, the level of precision will be diminished. To determine the maximum parameter value, one parameter was held constant while the other was adjusted to determine the parameter with the highest accuracy.

3.2 Reduced Error Pruning Tree

The REP Tree is an ensemble model consisting of the decision tree, and reduced error pruning (REP) approaches that are effective for classification and regression tasks [19]. One of the fastest decision tree classifier algorithms is the REP tree. It builds the decision tree utilizing the attribute's entropy and information gain, as well as a reduced error pruning strategy. It generates many trees and chooses the best one from the resulting list. The back fitting method is used by the REP tree to prune the tree. The REP tree algorithm sorts all numeric fields in the dataset only once at the start and then splits the attributes at each tree node using the sorted list. The numeric attributes are classified by minimizing total variance. The non-numeric properties are categorized using a regular decision tree and a reduced error pruning algorithm.

3.3 Performance Measures

The accuracy (*Acc*), Matthews correlation coefficient (*Mcc*), precision (*Prec*), recall (*Rec*), and F-score were used to evaluate the model's performance. Table 3 shows the performance metrics, together with their formulations and definitions, based on the confusion matrix described in Table 4. Fig. 3 depicts the methodology used in the development of the proposed models.

Table 3: Confusion matrix of binary problem

Actual condition	Predicted condition	
	Stable	Unstable
Stable	TP	FN
Unstable	FP	TN

Note: TP: true positives; TN: true negatives; FP: false positives; FN: false negatives.

Table 4: Definition and formulation of performance measures

Parameter	Definition	Formulation
Acc	Rate of correctly classified instances from total instances	$Acc = \frac{TP + TN}{TP + TN + FP + FN}$
Mcc	measure the difference between the predicted classes and actual classes	$Mcc = \frac{TP \times TN - FN \times FP}{\sqrt{(TP + FP)(TN + FP)(TN + FN)(TP + FN)}}$
Prec	Rate of correct predictions	$Prec = \frac{TP}{TP + FP} or \frac{TN}{TN + FN}$
Rec	True positive rate	$Rec = \frac{TP}{TP + FN} or \frac{TN}{TN + FP}$
F-score	Used to measure the accuracy of the experiment	$F - score = \frac{2 \times Prec \times Rec}{Prec + Rec}$

Note: *Acc*: accuracy; *Mcc*: matthews correlation coefficient; *Rec*: recall; *Prec*: precision.

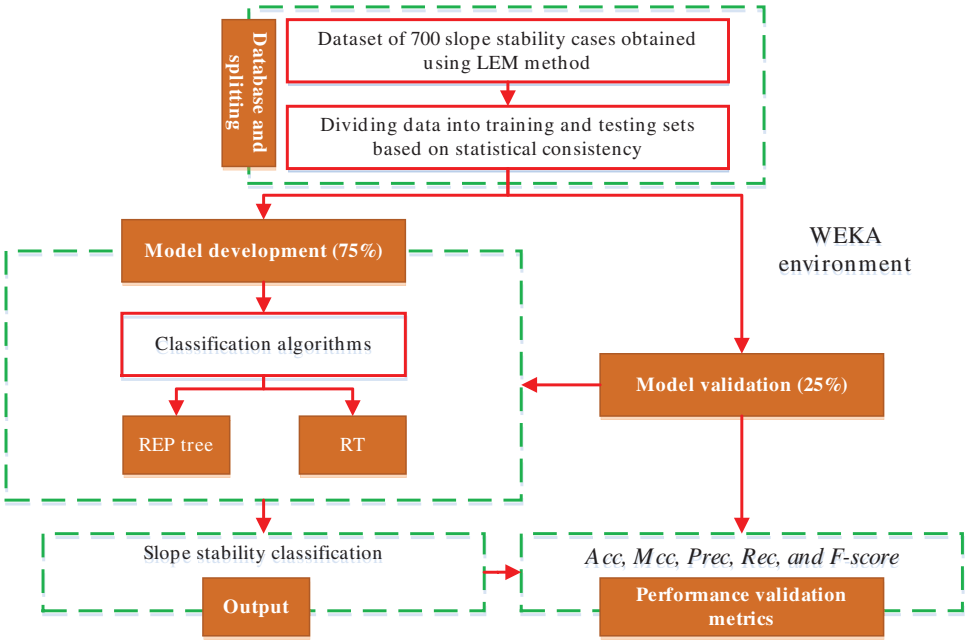

Figure 3: Flowchart depicting the general DT methodology

4 Results and Discussion

4.1 Construction of Models

In this section, two models using a random tree and REP tree to predict slope stability experience circular failure mode were developed. Researchers have used a different percentage of the available data as the training set for different problems. For instance, Kurup et al. [61] used 63% of the data for

training; Tang et al. [62] used 75%; while Padmini et al. [63] used 80%. In this study, 75% of the data was for training. The models were developed using Waikato Environment for Knowledge Analysis (WEKA) software [64]. WEKA is well-known and powerful data mining software developed at the New Zealand's University of Waikato. It is a set of open-source machine learning algorithms for data mining tasks in the real world data mining tasks, including classification, regression, and clustering, among others. For its prediction, the RT and REP tree algorithms were used. The minimum number of instances per leaf (n) is a key effective parameter for the accuracy of RT and REP tree models. The trial and error method is used in WEKA to get the best value for this parameter. It means that different values of n are used to train the RT and REP tree models, and the value that yields the best accuracy is chosen as the best. Fig. 4 depicts the RT and REP tree models. The RT and REP tree are 95 and 35, respectively. At each leaf node, the numbers in parentheses represent the total number of instances and the number of incorrectly classified cases. It is clear that some instances are misclassified in some leaves. The number of misclassified instances is specified after a slash. In order to create the most accurate model, the optimal values for n in WEKA were obtained through trial and error. The RT and REP tree models were trained using various values of n, with the best values for these parameters being 2 and 3, respectively. The RT algorithm's optimal value for K was 0.

4.2 Validation of Models

The performance of the models is validated using testing dataset that was not utilized during the model construction process. Validation is used to determine whether developed models may be generalized to conditions not experienced during the training phase. The results comparison of RT and REP tree models is shown in Table 5. Comparing the *Acc* and *Mcc*, the RT and REP tree models have the highest *Acc* and *Mcc*, whereas the RF model has the least value in the test phase. However, only the *Acc* and the *Mcc* cannot be used as indicators to judge the predictive performance for models. Therefore, stable and unstable classes are analyzed separately using *Prec*, *Rec*, and *F-score*. In the cases of stable class, the RT model has the highest *Prec*, and *F-score* comparison to the REPT model and the *Rec* values of RT and REP tree are at par, whereas the RF model presents the least value. Similarly, in the cases of unstable class, the RT model has the highest *Rec*, and *F-score* comparision to the REPT model and the *Prec* values of RT and REP tree are at par, whereas the RF model presents the least value. There are 5 and 8 unmatched prediction cases in the RT and REP tree models, respectively (see Fig. 4). In the test phase, the accuracy is 97.1429% and 95.4286%, respectively. These findings demonstrate that the developed RT and REP tree classification methods are useful and efficient in a practical point of view. Finally, the developed RT and REP tree models were compared to recently developed soft computing models in the literature to assess their accuracy. Table 5 shows the results of this comparison. Therefore, after comprehensive comparisons of the five measure indexes, the RT achieved a better prediction performance with ($Acc = 97.1429\%$, $Mcc = 0.935$, *F-score* for stable class $= 0.979$ and for unstable case *F-score* $= 0.935$) succeeded by the REP tree model with ($Acc = 95.4286\%$, $Mcc = 0.896$, *F-score* stable class $= 0.967$ and for unstable class *F-score* $= 0.923$) for the slope stability dataset in comparison to the AdaBoost ($Acc = 93.1429\%$, $Mcc = 0.830$, *F-score* for stable class $= 0.952$ and for unstable class *F-score* $= 0.878$) and RF ($Acc = 91.4286\%$, $Mcc = 0.794$, *F-score* $= 0.939$ and for unstable class *F-score* $= 0.854$) reported by Asteris et al. [55] for the test data. In general, the generalization and reliability of the developed models perform well, and a more balanced slope stability database can yield better prediction results. The primary advantage of the proposed models is a "white box" that reveals the clear relationship between input and output parameters. Consequently, using these models, the user (civil engineers) can easily compute slope stability.

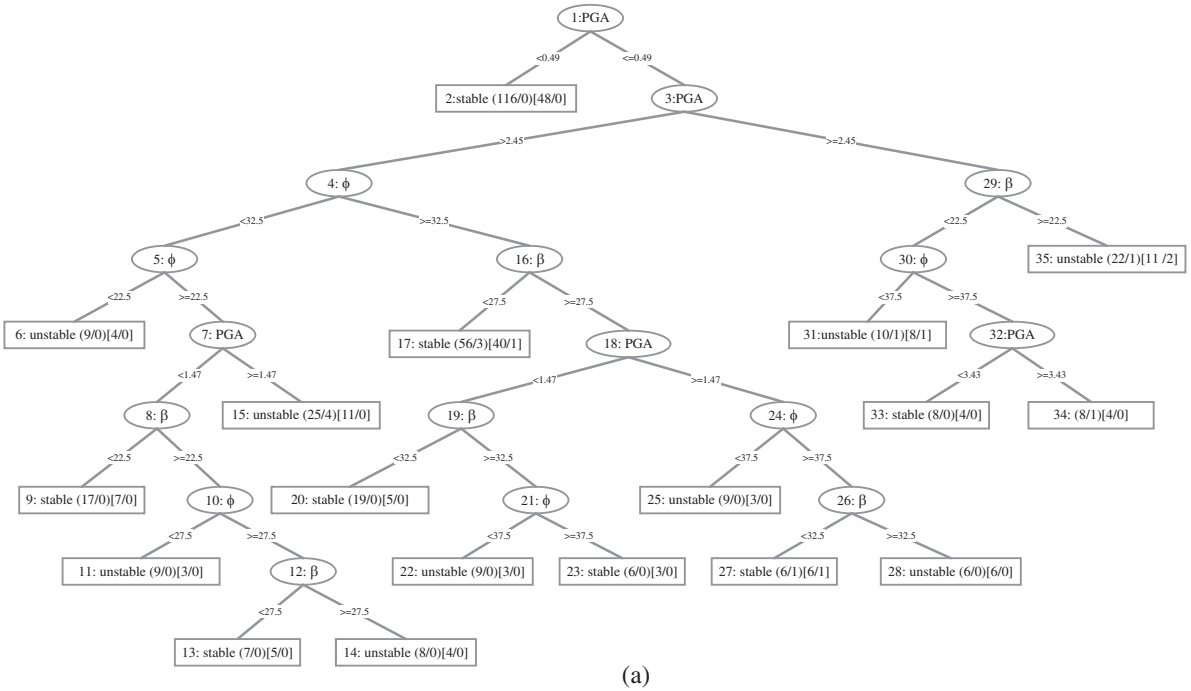

(a)

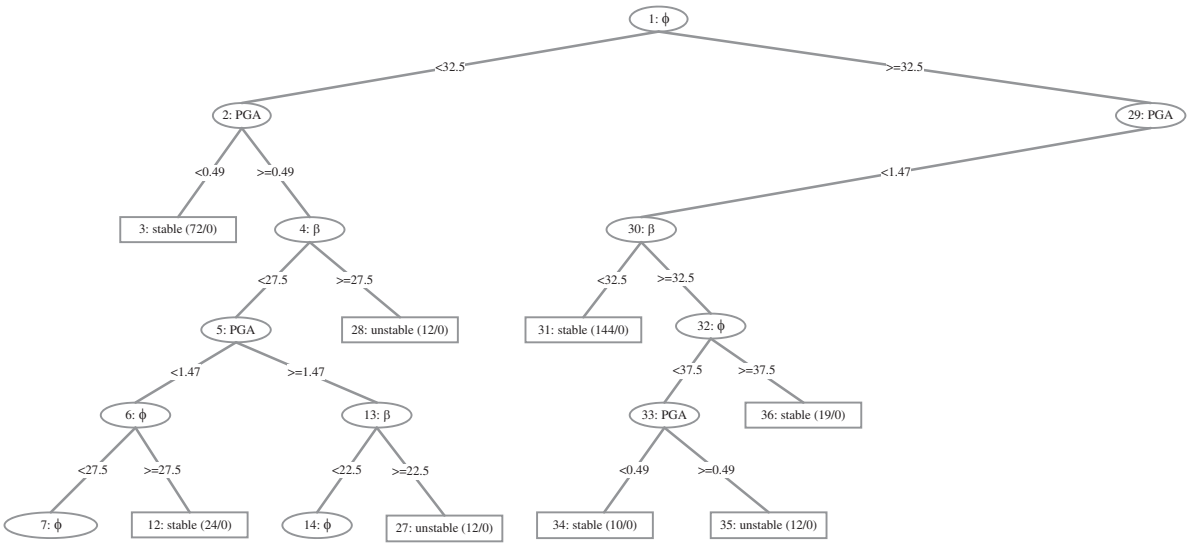

(b)

Figure 4: (a) REP tree and (b) part of RT

Table 5: Comparison of results obtained from different models

Model	Dataset	*Acc* (%)	*Mcc*	Stable			Unstable		
				Prec	*Rec*	*F*-score	*Prec*	*Rec*	*F-score*
RT	T	99.4286	0.987	0.994	0.997	0.996	0.994	0.988	0.991
	T∗	97.1429	0.935	0.960	1.000	0.979	1.000	0.911	0.935
REP tree	T	96.9524	0.931	0.983	0.972	0.977	0.942	0.964	0.953
	T∗	95.4286	0.896	0.937	1.000	0.967	1.000	0.857	0.923
AdaBoost [55]	T	100.000	1.000	1.000	1.000	1.000	1.000	1.000	1.000
	T∗	93.1429	0.830	0.945	0.960	0.952	0.896	0.860	0.878
RF [55]	T	97.7143	0.949	0.986	0.980	0.983	0.960	0.971	0.966
	T∗	91.4286	0.794	0.951	0.928	0.939	0.830	0.880	0.854

Note: T: training; T∗: testing.

Fig. 5 compares the classification results of the RT, REP tree, AdaBoost, and RF models from the testing phase to the FoS results obtained with the GeoStudio software for a better comparison. As previously indicated, each model in the testing phase used 175 data samples, which constituted for 25% of the total data. Fig. 4 shows that the RT and REP tree techniques were able to achieve excellent results with the lowest number of unmatched cases. For RT, REP tree, AdaBoost, and RF, the matched and unmatched numbers were 170 and 5,167 and 8, 163 and 12, and 160 and 15, respectively, indicating the RT model's superiority over the REP tree and other models reported in the literature for slope stability classification. The error rate throughout the testing phase was low, illustrating the RT model's high performance. It was determined that the model with the best performance for slope stability classification was the RT, and that it could be utilized in this field for the same purpose of minimizing the associated risk.

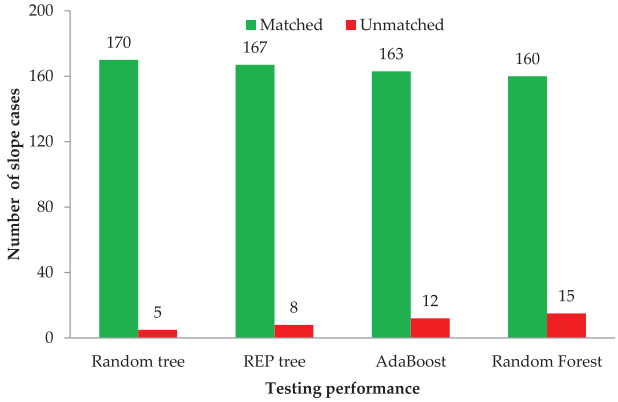

Figure 5: Comparison of results obtained from different models

4.3 Rank Analysis

The rank analysis is the easiest and most extensively used method for evaluating and comparing the effectiveness of developed models. In this study, the statistical parameters are employed to

determine the score value, with their ideal values serving as a benchmark. It is dependent on the number of models used. The best performing outcomes model receives the highest score, and vice versa. Two models with the same outcomes may have the same ranking ratings.

Table 6 compares the testing stage results obtained by the indicators: i.e., *Acc*, *Mcc*, *Prec*, *Rec*, and *F-score*. The score attained by RT is the highest in the testing phase (19), followed by the REP tree (13) and AdaBoost (10), and RF attains the most negligible score value in the testing phase (7). Except for the recall, RT achieved better accuracy and performance than the REP tree, AdaBoost, and RF models. It can be inferred from the rank values that the RT model has performances superior to the REP tree, AdaBoost, and RF and is the clear winner in terms of performance to the other applied models.

Table 6: Rank analysis of the developed models for slope stability classification outcomes for testing dataset

Model statistical parameters		RT	REP tree	AdaBoost [55]	RF [55]
Acc (%)	Value	97.1429	95.4286	93.1429	91.4286
	Rank	4	3	2	1
Mcc	Value	0.935	0.896	0.830	0.794
	Rank	4	3	2	1
Prec	Value	0.960	0.937	0.945	0.951
	Rank	4	1	2	3
Rec	Value	1.000	1.000	0.960	0.928
	Rank	3	3	2	1
F-score	Value	0.979	0.967	0.952	0.939
	Rank	4	3	2	1
Total		19	13	10	7

5 Conclusions

In this paper, a RT and REP tree models were applied to classify the stability of 700 slopes (464 stable slopes and 236 unstable slopes) under seismic conditions, which were modeled and analyzed in GeoStudio software. The variables of H, β, c, ϕ, and PGA were set as model inputs for the classification of slopes where FoS ≥ 1 and FoS < 1 were considered for stable and unstable slopes, respectively. To quantify the performance of the RT and REP tree models, accuracy, Matthews correlation coefficient, precision, recall, and *F-score*, performance indices were computed for both training and testing stages.

The following are the main important findings of this study:

1. The outcome of the developed models is two slope stability graphs that are very easy to use and do not require extensive training. Unlike most soft computing methods, these models explicitly

indicate the relationship between input and output parameters. Based on the findings, these relationships are consistent with intuition and engineering judgment.

2. The RT and REP tree models classification accuracy in the test phase is 97.1429% and 95.4286%, respectively, demonstrating that both models are useful and efficient in practice. In addition, the Matthews correlation coefficient near to +1 indicates high values shows good agreement between actual and predicted classes.
3. Comparing models' performance reveals that the RT model gives more accurate classifications than the REP tree model.
4. Compared to the random forest and AdaBoost models in the literature, the presented models have a better ability for prediction, and their use is facilitated by a clear graphical output.

Future research should utilize a more balanced slope stability database to evaluate the models' reliability in predicting slope stability. Although the proposed models produce desired predictions and performed well with *Acc* greater than 95%, Additional rocks' depth, soil type, and rainfall factors can all be considered in these models to improve the generalization and reliability.

Funding Statement: The work was supported by the National Key Research and Development Plan of China under Grant No. 2021YFB2600703.

Availability of Data and Materials: The authors declare that all data supporting the findings of this study are available within the article.

Conflicts of Interest: The authors declare that they have no conflicts of interest to report regarding the present study.

References

1. Sakellariou, M., Ferentinou, M. (2005). A study of slope stability prediction using neural networks. *Geotechnical & Geological Engineering, 23(4),* 419–445. https://doi.org/10.1007/s10706-004-8680-5
2. Duncan, J. M. (2000). Factors of safety and reliability in geotechnical engineering. *Journal of Geotechnical and Geoenvironmental Engineering, 126(4),* 307–316. 10.1061/(ASCE)1090-0241(2000)126:4(307)
3. Suman, S., Khan, S., Das, S., Chand, S. (2016). Slope stability analysis using artificial intelligence techniques. *Natural Hazards, 84(2),* 727–748. https://doi.org/10.1007/s11069-016-2454-2
4. Thiebes, B., Bell, R., Glade, T., Jäger, S., Mayer, J. et al. (2014). Integration of a limit-equilibrium model into a landslide early warning system. *Landslides, 11(5),* 859–875. https://doi.org/10.1007/s10346-013-0416-2
5. Verma, D., Kainthola, A., Gupte, S., Singh, T. (2013). A finite element approach of stability analysis of internal dump slope in Wardha valley coal field, India, Maharashtra. *American Journal of Mining and Metallurgy, 1(1),* 1–6.
6. Cai, F., Ugai, K. (2004). Numerical analysis of rainfall effects on slope stability. *International Journal of Geomechanics, 4(2),* 69–78. https://doi.org/10.1061/(ASCE)1532-3641(2004)4:2(69)
7. Dawson, E., Roth, W. H., Drescher, A. (1999). Slope stability analysis by strength reduction. *Géoteclinique, 49(6),* 835–840. https://doi.org/10.1680/geot.1999.49.6.835
8. Griffiths, D., Lane, P. (1999). Slope stability analysis by finite elements. *Geotechnique, 49(3),* 387–403. https://doi.org/10.1680/geot.1999.49.3.387

9. Liu, Z., Shao, J., Xu, W., Chen, H., Zhang, Y. (2014). An extreme learning machine approach for slope stability evaluation and prediction. *Natural Hazards, 73(2),* 787–804. 10.1007/s11069-014-1106-7
10. Xue, X. (2017). Prediction of slope stability based on hybrid PSO and LSSVM. *Journal of Computing in Civil Engineering, 31(1),* 04016041. https://doi.org/10.1061/(ASCE)CP.1943-5487.0000607
11. Bye, A., Bell, F. (2001). Stability assessment and slope design at sandsloot open pit, South Africa. *International Journal of Rock Mechanics and Mining Sciences, 38(3),* 449–466. https://doi.org/10.1016/S1365-1609(01)00014-4
12. Taheri, A., Tani, K. (2010). Assessment of the stability of rock slopes by the slope stability rating classification system. *Rock Mechanics and Rock Engineering, 43(3),* 321–333. https://doi.org/10.1007/s00603-009-0050-4
13. Chen, W. F., Baladi, G. Y. (1985). *Soil plasticity: Theory and implementation*. AE, Amsterdam, The Netherlands: Elsevier Science Publisher.
14. Lechman, J., Griffiths, D. (2000). Analysis of the progression of failure of earth slopes by finite elements. In: *Slope stability*, pp. 250–265. Denver, Colorado, USA.
15. Ahmad, M., Tang, X. W., Qiu, J. N., Gu, W. J., Ahmad, F. (2020). A hybrid approach for evaluating CPT-based seismic soil liquefaction potential using bayesian belief networks. *Journal of Central South University, 27(2),* 500–516. https://doi.org/10.1007/s11771-020-4312-3
16. Ahmad, M., Tang, X. W., Qiu, J. N., Ahmad, F. (2019). Evaluating seismic soil liquefaction potential using Bayesian belief network and C4.5 decision tree approaches. *Applied Sciences, 9(20),* 4226. https://doi.org/10.3390/app9204226
17. Ahmad, M., Tang, X., Qiu, J., Ahmad, F., Gu, W. (2019). LLDV-A comprehensive framework for assessing the effects of liquefaction land damage potential. *2019 IEEE 14th International Conference on Intelligent Systems and Knowledge Engineering (ISKE)*, pp. 527–533. Dalian, China, IEEE.
18. Ahmad, M., Tang, X. W., Qiu, J. N., Ahmad, F., Gu, W. J. (2020). A step forward towards a comprehensive framework for assessing liquefaction land damage vulnerability: Exploration from historical data. *Frontiers of Structural and Civil Engineering, 14(6),* 1476–1491. https://doi.org/10.1007/s11709-020-0670-z
19. Ahmad, M., Tang, X., Ahmad, F. (2020). Evaluation of liquefaction-induced settlement using random forest and REP tree models: Taking Pohang earthquake as a case of illustration. In: *Natural hazards-impacts, adjustments & resilience*. London, UK: IntechOpen.
20. Ahmad, M., Al-Shayea, N. A., Tang, X. W., Jamal, A., M Al-Ahmadi, H. et al. (2020). Predicting the pillar stability of underground mines with random trees and C4.5 decision trees. *Applied Sciences, 10(18),* 6486. https://doi.org/10.3390/app10186486
21. Ahmad, M., Kamiński, P., Olczak, P., Alam, M., Iqbal, M. J. et al. (2021). Development of prediction models for shear strength of rockfill material using machine learning techniques. *Applied Sciences, 11(13),* 6167. https://doi.org/10.3390/app11136167
22. Noori, A. M., Mikaeil, R., Mokhtarian, M., Haghshenas, S. S., Foroughi, M. (2020). Feasibility of intelligent models for prediction of utilization factor of TBM. *Geotechnical and Geological Engineering, 38(3),* 3125–3143. https://doi.org/10.1007/s10706-020-01213-9
23. Dormishi, A., Ataei, M., Mikaeil, R., Khalokakaei, R., Haghshenas, S. S. (2019). Evaluation of gang saws' performance in the carbonate rock cutting process using feasibility of intelligent approaches. *Engineering Science and Technology, an International Journal, 22(3),* 990–1000. https://doi.org/10.1016/j.jestch.2019.01.007
24. Mikaeil, R., Haghshenas, S. S., Hoseinie, S. H. (2018). Rock penetrability classification using artificial bee colony (ABC) algorithm and self-organizing map. *Geotechnical and Geological Engineering, 36(2),* 1309–1318.
25. Mikaeil, R., Haghshenas, S. S., Ozcelik, Y., Gharehgheshlagh, H. H. (2018). Performance evaluation of adaptive neuro-fuzzy inference system and group method of data handling-type neural network for

estimating wear rate of diamond wire saw. *Geotechnical and Geological Engineering, 36(6),* 3779–3791. https://doi.org/10.1007/s10706-018-0571-2

26. Momeni, E., Nazir, R., Armaghani, D. J., Maizir, H. (2014). Prediction of pile bearing capacity using a hybrid genetic algorithm-based ANN. *Measurement, 57,* 122–131. https://doi.org/10.1016/j.measurement.2014.08.007
27. Xie, C., Nguyen, H., Choi, Y., Armaghani, D. J. (2022). Optimized functional linked neural network for predicting diaphragm wall deflection induced by braced excavations in clays. *Geoscience Frontiers, 13(2),* 101313. https://doi.org/10.1016/j.gsf.2021.101313
28. Armaghani, D. J., Mohamad, E. T., Narayanasamy, M. S., Narita, N., Yagiz, S. (2017). Development of hybrid intelligent models for predicting TBM penetration rate in hard rock condition. *Tunnelling and Underground Space Technology, 63,* 29–43. https://doi.org/10.1016/j.tust.2016.12.009
29. Yan, T., Shen, S. L., Zhou, A. (2023). Identification of geological characteristics from construction parameters during shield tunnelling. *Acta Geotechnica, 18(1),* 535–551. https://doi.org/10.1007/s11440-022-01590-w
30. Amjad, M., Ahmad, I., Ahmad, M., Wróblewski, P., Kamiński, P. et al. (2022). Prediction of pile bearing capacity using XGBoost algorithm: Modeling and performance evaluation. *Applied Sciences, 12(4),* 2126. https://doi.org/10.3390/app12042126
31. Ahmad, M., Al-Mansob, R. A., Kashyzadeh, K. R., Keawsawasvong, S., Sabri Sabri, M. M. et al. (2022). Extreme gradient boosting algorithm for predicting shear strengths of rockfill materials. *Complexity, 2022,* 9415863. https://doi.org/10.1155/2022/9415863
32. Hasanipanah, M., Jamei, M., Mohammed, A. S., Amar, M. N., Hocine, O. et al. (2022). Intelligent prediction of rock mass deformation modulus through three optimized cascaded forward neural network models. *Earth Science Informatics, 15(3),* 1659–1669. https://doi.org/10.1007/s12145-022-00823-6
33. Hasanipanah, M., Monjezi, M., Shahnazar, A., Armaghani, D. J., Farazmand, A. (2015). Feasibility of indirect determination of blast induced ground vibration based on support vector machine. *Measurement, 75,* 289–297. https://doi.org/10.1016/j.measurement.2015.07.019
34. Koopialipoor, M., Jahed Armaghani, D., Hedayat, A., Marto, A., Gordan, B. (2019). Applying various hybrid intelligent systems to evaluate and predict slope stability under static and dynamic conditions. *Soft Computing, 23(14),* 5913–5929. https://doi.org/10.1007/s00500-018-3253-3
35. Mahdiyar, A., Hasanipanah, M., Armaghani, D. J., Gordan, B., Abdullah, A. et al. (2017). A monte carlo technique in safety assessment of slope under seismic condition. *Engineering with Computers, 33(4),* 807–817. https://doi.org/10.1007/s00366-016-0499-1
36. Gordan, B., Jahed Armaghani, D., Hajihassani, M., Monjezi, M. (2016). Prediction of seismic slope stability through combination of particle swarm optimization and neural network. *Engineering with Computers, 32(1),* 85–97. https://doi.org/10.1007/s00366-015-0400-7
37. Alimohammadlou, Y., Najafi, A., Gokceoglu, C. (2014). Estimation of rainfall-induced landslides using ANN and fuzzy clustering methods: A case study in saeen slope, Azerbaijan Province, Iran. *Catena, 120,* 149–162. https://doi.org/10.1016/j.catena.2014.04.009
38. Erzin, Y., Cetin, T. (2013). The prediction of the critical factor of safety of homogeneous finite slopes using neural networks and multiple regressions. *Computers & Geosciences, 51,* 305–313. https://doi.org/10.1016/j.cageo.2012.09.003
39. Samui, P., Bhattacharya, G., Das, S. K. (2008). Support vector machine and relevance vector machine classifier in analysis of slopes. In: *International association for computer methods and advances in geomechanics (IACMAG)*, pp. 1–6. Goa, India.
40. Feng, X. T. (2000). Introduction of intelligent rock mechanics. In: *Science*. Beijing, China: Science Press.
41. Lu, P., Rosenbaum, M. (2003). Artificial neural networks and grey systems for the prediction of slope stability. *Natural Hazards, 30(3),* 383–398. https://doi.org/10.1023/B:NHAZ.0000007168.00673.27

42. Li, X. (2004). *Comparative studies of artificial neural networks and adaptive neuro-fuzzy inference system based approach for the circular sliding slopes stability analysis (Doctoral Dissertation)*. University of South China.
43. Huang, Z. Q., Cui, J., Liu, H. (2004). Chaotic neural network method for slope stability prediction. *Chinese Journal of Rock Mechanics and Engineering, 22,* 015.
44. Wang, H., Xu, W., Xu, R. (2005). Slope stability evaluation using back propagation neural networks. *Engineering Geology, 80(3–4),* 302–315. https://doi.org/10.1016/j.enggeo.2005.06.005
45. Samui, P. (2008). Slope stability analysis: A support vector machine approach. *Environmental Geology, 56(2),* 255–267. https://doi.org/10.1007/s00254-007-1161-4
46. Zhao, H. B. (2008). Slope reliability analysis using a support vector machine. *Computers and Geotechnics, 35(3),* 459–467. https://doi.org/10.1016/j.compgeo.2007.08.002
47. Choobbasti, A., Farrokhzad, F., Barari, A. (2009). Prediction of slope stability using artificial neural network (case study: Noabad, Mazandaran, Iran). *Arabian Journal of Geosciences, 2(4),* 311–319. https://doi.org/10.1007/s12517-009-0035-3
48. Das, S. K., Biswal, R. K., Sivakugan, N., Das, B. (2011). Classification of slopes and prediction of factor of safety using differential evolution neural networks. *Environmental Earth Sciences, 64(1),* 201–210. https://doi.org/10.1007/s12665-010-0839-1
49. Hoang, N. D., Pham, A. D. (2016). Hybrid artificial intelligence approach based on metaheuristic and machine learning for slope stability assessment: A multinational data analysis. *Expert Systems with Applications, 46,* 60–68. https://doi.org/10.1016/j.eswa.2015.10.020
50. Verma, A., Singh, T., Chauhan, N. K., Sarkar, K. (2016). A hybrid FEM–ANN approach for slope instability prediction. *Journal of the Institution of Engineers (India): Series A, 97(3),* 171–180. https://doi.org/10.1007/s40030-016-0168-9
51. Rukhaiyar, S., Alam, M., Samadhiya, N. K. (2018). A PSO-ANN hybrid model for predicting factor of safety of slope. *International Journal of Geotechnical Engineering, 12(6),* 556–566.
52. Feng, X., Li, S., Yuan, C., Zeng, P., Sun, Y. (2018). Prediction of slope stability using naive Bayes classifier. *KSCE Journal of Civil Engineering, 22(3),* 941–950. https://doi.org/10.1007/s12205-018-1337-3
53. Zhou, J., Li, E., Yang, S., Wang, M., Shi, X. et al. (2019). Slope stability prediction for circular mode failure using gradient boosting machine approach based on an updated database of case histories. *Safety Science, 118,* 505–518. https://doi.org/10.1016/j.ssci.2019.05.046
54. Ahmad, F., Tang, X. W., Qiu, J. N., Wróblewski, P., Ahmad, M. et al. (2022). Prediction of slope stability using tree augmented naive-bayes classifier: Modeling and performance evaluation. *Mathematical Biosciences and Engineering, 19,* 4526–4546. https://doi.org/10.3934/mbe.2022209
55. Asteris, P. G., Rizal, F. I. M., Koopialipoor, M., Roussis, P. C., Ferentinou, M. et al. (2012). Slope stability classification under seismic conditions using several tree-based intelligent techniques. *Applied Sciences, 12(3),* 1753. https://doi.org/10.3390/app12031753
56. Kiranmai, S. A., Laxmi, A. J. (2018). Data mining for classification of power quality problems using WEKA and the effect of attributes on classification accuracy. *Protection and Control of Modern Power Systems, 3(1),* 29. https://doi.org/10.1186/s41601-018-0103-3
57. Kramer, S. (1996). *Geotechnical earthquake engineering*, New Jersey: Prentice Hall Upper Saddle River.
58. Kalmegh, S., (2015). Analysis of weka data mining algorithm reptree, simple cart and randomtree for classification of Indian news. *International Journal of Innovative Science, Engineering & Technology, 2(2),* 438–446.
59. Hamsagayathri, P., Sampath, P. (2017). Performance analysis of breast cancer classification using decision tree classifiers. *International Journal of Current Pharmaceutical Research, 9(2),* 19–25. https://doi.org/10.22159/ijcpr.2017v9i2.17383

60. Witten, I., Frank, E., Hall, M. (2011). *Data mining: Practical machine learning tools and techniques*, 3rd edition. San Francisco: Morgan Kaufmann.
61. Kurup, P. U., Dudani, N. K. (2002). Neural networks for profiling stress history of clays from PCPT data. *Journal of Geotechnical and Geoenvironmental Engineering, 128(7),* 569–579. https://doi.org/10.1061/(ASCE)1090-0241(2002)128:7(569)
62. Tang, Y., Zhang, Y. Q., Huang, Z., Hu, X. (2005). Granular SVM-RFE gene selection algorithm for reliable prostate cancer classification on microarray expression data. *Fifth IEEE Symposium on Bioinformatics and Bioengineering (BIBE'05)*, Minneapolis, Minnesota, IEEE.
63. Padmini, D., Ilamparuthi, K., Sudheer, K. (2008). Ultimate bearing capacity prediction of shallow foundations on cohesionless soils using neurofuzzy models. *Computers and Geotechnics, 35(1),* 33–46. https://doi.org/10.1016/j.compgeo.2007.03.001
64. Witten, I. H., Frank, E., Hall, M. (2005). *Data mining: Practical machine learning tools and techniques*. San Francisco: Morgen Kaufmann.

Appendix A

Table A1: Dataset used to construct and validate the model

S. No.	H/m	$\beta/°$	c/kPa	$\phi/°$	PGA/ms^{-2}	FoS
1	15	20	20	20	0	1.063
2	15	20	20	20	0.981	0.803
3	15	20	20	25	0	1.355
4	15	20	20	25	0.981	1.022
5	15	20	20	25	1.962	0.81
6	15	20	20	30	0	1.671
7	15	20	20	30	0.981	1.261
8	15	20	20	30	1.962	0.998
9	15	20	20	35	0	2.02
10	15	20	20	35	0.981	1.524
11	15	20	20	35	1.962	1.206
12	15	20	20	35	2.943	0.986
13	15	20	20	40	0	2.414
14	15	20	20	40	0.981	1.821
15	15	20	20	40	1.962	1.442
16	15	20	20	40	2.943	1.178
17	15	20	20	40	3.924	0.984
18	15	20	30	20	0	1.076
19	15	20	30	20	0.981	0.812
20	15	20	30	25	0	1.368
21	15	20	30	25	0.981	1.033
22	15	20	30	25	1.962	0.818
23	15	20	30	30	0	1.685
24	15	20	30	30	0.981	1.271
25	15	20	30	30	1.962	1.007
26	15	20	30	30	2.943	0.823

(Continued)

Table A1 (continued)

S. No.	H/m	$\beta/°$	c/kPa	$\phi/°$	PGA/ms^{-2}	FoS
27	15	20	30	35	0	2.034
28	15	20	30	35	0.981	1.535
29	15	20	30	35	1.962	1.216
30	15	20	30	35	2.943	0.994
31	15	20	30	40	0	2.43
32	15	20	30	40	0.981	1.883
33	15	20	30	40	1.962	1.452
34	15	20	30	40	2.943	1.186
35	15	20	30	40	3.924	0.991
36	15	20	40	20	0	1.087
37	15	20	40	20	0.981	0.821
38	15	20	40	25	0	1.38
39	15	20	40	25	0.981	1.042
40	15	20	40	25	1.962	0.826
41	15	20	40	30	0	1.698
42	15	20	40	30	0.981	1.282
43	15	20	40	30	1.962	1.015
44	15	20	40	30	2.943	0.83
45	15	20	40	35	0	2.048
46	15	20	40	35	0.981	1.546
47	15	20	40	35	1.962	1.224
48	15	20	40	35	2.943	1.001
49	15	20	40	35	3.924	0.837
50	15	20	40	40	0	2.443
51	15	20	40	40	0.981	1.844
52	15	20	40	40	1.962	1.46
53	15	20	40	40	2.943	1.194
54	15	20	40	40	3.924	0.998
55	15	20	50	20	0	1.097
56	15	20	50	20	0.981	0.829
57	15	20	50	25	0	1.391
58	15	20	50	25	0.981	1.051
59	15	20	50	25	1.962	0.833
60	15	20	50	30	0	1.71
61	15	20	50	30	0.981	1.291
62	15	20	50	30	1.962	1.023
63	15	20	50	30	2.943	0.837
64	15	20	50	35	0	2.061
65	15	20	50	35	0.981	1.556
66	15	20	50	35	1.962	1.233
67	15	20	50	35	2.943	1.008

(Continued)

Table A1 (continued)

S. No.	H/m	$\beta/°$	c/kPa	$\phi/°$	PGA/ms^{-2}	FoS
68	15	20	50	35	3.924	0.843
69	15	20	50	40	0	2.457
70	15	20	50	40	0.981	1.855
71	15	20	50	40	1.962	1.469
72	15	20	50	40	2.943	1.201
73	15	20	50	40	3.924	1.004
74	15	25	20	25	0	1.057
75	15	25	20	25	0.981	0.831
76	15	25	20	30	0	1.301
77	15	25	20	30	0.981	1.023
78	15	25	20	30	1.962	0.829
79	15	25	20	35	0	1.572
80	15	25	20	35	0.981	1.235
81	15	25	20	35	1.962	1.001
82	15	25	20	35	2.943	0.828
83	15	25	20	40	0	1.877
84	15	25	20	40	0.981	1.475
85	15	25	20	40	1.962	1.195
86	15	25	20	40	2.943	0.989
87	15	25	30	25	0	1.069
88	15	25	30	25	0.981	0.842
89	15	25	30	30	0	1.315
90	15	25	30	30	0.981	1.035
91	15	25	30	30	1.962	0.839
92	15	25	30	35	0	1.586
93	15	25	30	35	0.981	1.248
94	15	25	30	35	1.962	1.012
95	15	25	30	35	2.943	0.838
96	15	25	30	40	0	1.893
97	15	25	30	40	0.981	1.488
98	15	25	30	40	1.962	1.206
99	15	25	30	40	2.943	0.999
100	15	25	40	25	0	1.081
101	15	25	40	25	0.981	0.851
102	15	25	40	30	0	1.327
103	15	25	40	30	0.981	1.045
104	15	25	40	30	1.962	0.848
105	15	25	40	35	0	1.599
106	15	25	40	35	0.981	1.258
107	15	25	40	35	1.962	1.021
108	15	25	40	35	2.943	0.846

(Continued)

Table A1 (continued)

S. No.	H/m	$\beta/°$	c/kPa	$\phi/°$	PGA/ms^{-2}	FoS
109	15	25	40	40	0	1.907
110	15	25	40	40	0.981	1.5
111	15	25	40	40	1.962	1.216
112	15	25	40	40	2.943	1.007
113	15	25	40	40	3.924	0.847
114	15	25	50	25	0	1.091
115	15	25	50	25	0.981	0.859
116	15	25	50	30	0	1.338
117	15	25	50	30	0.981	1.054
118	15	25	50	30	1.962	0.856
119	15	25	50	35	0	1.612
120	15	25	50	35	0.981	1.268
121	15	25	50	35	1.962	1.029
122	15	25	50	35	2.943	0.853
123	15	25	50	40	0	1.919
124	15	25	50	40	0.981	1.51
125	15	25	50	40	1.962	1.225
126	15	25	50	40	2.943	1.015
127	15	25	50	40	3.924	0.854
128	15	30	20	30	0	1.054
129	15	30	20	30	0.981	0.851
130	15	30	20	35	0	1.272
131	15	30	20	35	0.981	1.026
132	15	30	20	35	1.962	0.843
133	15	30	20	40	0	1.517
134	15	30	20	40	0.981	1.223
135	15	30	20	40	1.962	1.006
136	15	30	20	40	2.943	0.838
137	15	30	30	30	0	1.068
138	15	30	30	30	0.981	0.862
139	15	30	30	35	0	1.287
140	15	30	30	35	0.981	1.038
141	15	30	30	35	1.962	0.854
142	15	30	30	40	0	1.534
143	15	30	30	40	0.981	1.237
144	15	30	30	40	1.962	1.018
145	15	30	30	40	2.943	0.849
146	15	30	40	30	0	1.08
147	15	30	40	30	0.981	0.872
148	15	30	40	35	0	1.299
149	15	30	40	35	0.981	1.049

(Continued)

Table A1 (continued)

S. No.	H/m	$\beta/°$	c/kPa	$\phi/°$	PGA/ms^{-2}	FoS
150	15	30	40	35	1.962	0.864
151	15	30	40	40	0	1.547
152	15	30	40	40	0.981	1.249
153	15	30	40	40	1.962	1.028
154	15	30	40	40	2.943	0.858
155	15	30	50	30	0	1.091
156	15	30	50	30	0.981	0.882
157	15	30	50	35	0	1.311
158	15	30	50	35	0.981	1.059
159	15	30	50	35	1.962	0.873
160	15	30	50	40	0	1.56
161	15	30	50	40	0.981	1.26
162	15	30	50	40	1.962	1.037
163	15	30	50	40	2.943	0.866
164	15	35	20	35	0	1.041
165	15	35	20	35	0.981	0.854
166	15	35	20	40	0	1.237
167	15	35	20	40	0.981	1.013
168	15	35	20	40	1.962	0.839
169	15	35	30	35	0	1.055
170	15	35	30	35	0.981	0.867
171	15	35	30	40	0	1.25
172	15	35	30	40	0.981	1.028
173	15	35	30	40	1.962	0.852
174	15	35	40	35	0	1.299
175	15	35	40	35	0.981	0.878
176	15	35	40	40	0	1.547
177	15	35	40	40	0.981	1.04
178	15	35	40	40	1.962	0.864
179	15	35	50	35	0	1.311
180	15	35	50	35	0.981	0.888
181	15	35	50	40	0	1.56
182	15	35	50	40	0.981	1.051
183	15	35	50	40	1.962	0.875
184	20	20	20	20	0	1.037
185	20	20	20	20	0.981	0.785
186	20	20	20	25	0	1.323
187	20	20	20	25	0.981	1.001
188	20	20	20	25	1.962	0.794
189	20	20	20	30	0	1.632
190	20	20	20	30	0.981	1.235

(Continued)

Table A1 (continued)

S. No.	H/m	$\beta/°$	c/kPa	$\phi/°$	PGA/ms^{-2}	FoS
191	20	20	20	30	1.962	0.979
192	20	20	20	35	0	1.973
193	20	20	20	35	0.981	1.493
194	20	20	20	35	1.962	1.184
195	20	20	20	35	2.943	0.968
196	20	20	20	40	0	2.359
197	20	20	20	40	0.981	1.785
198	20	20	20	40	1.962	1.415
199	20	20	20	40	2.943	1.157
200	20	20	20	40	3.924	0.966
201	20	20	30	20	0	1.048
202	20	20	30	20	0.981	0.793
203	20	20	30	25	0	1.334
204	20	20	30	25	0.981	1.01
205	20	20	30	25	1.962	0.801
206	20	20	30	30	0	1.644
207	20	20	30	30	0.981	1.244
208	20	20	30	30	1.962	0.987
209	20	20	30	35	0	1.987
210	20	20	30	35	0.981	1.504
211	20	20	30	35	1.962	1.192
212	20	20	30	35	2.943	0.975
213	20	20	30	40	0	2.373
214	20	20	30	40	0.981	1.796
215	20	20	30	40	1.962	1.424
216	20	20	30	40	2.943	1.165
217	20	20	30	40	3.924	0.973
218	20	20	40	20	0	1.057
219	20	20	40	20	0.981	0.801
220	20	20	40	25	0	1.344
221	20	20	40	25	0.981	1.018
222	20	20	40	25	1.962	0.808
223	20	20	40	30	0	1.654
224	20	20	40	30	0.981	1.253
225	20	20	40	30	1.962	0.994
226	20	20	40	35	0	1.988
227	20	20	40	35	0.981	1.512
228	20	20	40	35	1.962	1.2
229	20	20	40	35	2.943	0.981
230	20	20	40	40	0	2.385
231	20	20	40	40	0.981	1.806

(Continued)

Table A1 (continued)

S. No.	H/m	$\beta/°$	c/kPa	$\phi/°$	PGA/ms^{-2}	FoS
232	20	20	40	40	1.962	1.432
233	20	20	40	40	2.943	1.171
234	20	20	40	40	3.924	0.979
235	20	20	50	20	0	1.065
236	20	20	50	20	0.981	0.807
237	20	20	50	25	0	1.353
238	20	20	50	25	0.981	1.025
239	20	20	50	25	1.962	0.813
240	20	20	50	30	0	1.664
241	20	20	50	30	0.981	1.26
242	20	20	50	30	1.962	1
243	20	20	50	30	2.943	0.819
244	20	20	50	35	0	2.008
245	20	20	50	35	0.981	1.521
246	20	20	50	35	1.962	1.207
247	20	20	50	35	2.943	0.987
248	20	20	50	40	0	2.396
249	20	20	50	40	0.981	1.814
250	20	20	50	40	1.962	1.439
251	20	20	50	40	2.943	1.177
252	20	20	50	40	3.924	0.984
253	20	25	20	25	0	1.043
254	20	25	20	25	0.981	0.821
255	20	25	20	30	0	1.286
256	20	25	20	30	0.981	1.012
257	20	25	20	30	1.962	0.82
258	20	25	20	35	0	1.555
259	20	25	20	35	0.981	1.223
260	20	25	20	35	1.962	0.992
261	20	25	20	40	0	1.858
262	20	25	20	40	0.981	1.461
263	20	25	20	40	1.962	1.184
264	20	25	20	40	2.943	0.98
265	20	25	30	25	0	1.054
266	20	25	30	25	0.981	0.83
267	20	25	30	30	0	1.297
268	20	25	30	30	0.981	1.021
269	20	25	30	30	1.962	0.828
270	20	25	30	35	0	1.566
271	20	25	30	35	0.981	1.232
272	20	25	30	35	1.962	0.999

(Continued)

Table A1 (continued)

S. No.	H/m	$\beta/°$	c/kPa	$\phi/°$	PGA/ms^{-2}	FoS
273	20	25	30	40	0	1.87
274	20	25	30	40	0.981	1.472
275	20	25	30	40	1.962	1.193
276	20	25	30	40	2.943	0.988
277	20	25	40	25	0	1.063
278	20	25	40	25	0.981	0.837
279	20	25	40	30	0	1.308
280	20	25	40	30	0.981	1.03
281	20	25	40	30	1.962	0.835
282	20	25	40	35	0	1.577
283	20	25	40	35	0.981	1.241
284	20	25	40	35	1.962	1.007
285	20	25	40	35	2.943	0.834
286	20	25	40	40	0	1.881
287	20	25	40	40	0.981	1.48
288	20	25	40	40	1.962	1.201
289	20	25	40	40	2.943	0.994
290	20	25	50	25	0	1.072
291	20	25	50	25	0.981	0.845
292	20	25	50	30	0	1.317
293	20	25	50	30	0.981	1.037
294	20	25	50	30	1.962	0.842
295	20	25	50	35	0	1.587
296	20	25	50	35	0.981	1.25
297	20	25	50	35	1.962	1.014
298	20	25	50	35	2.943	0.84
299	20	25	50	40	0	1.892
300	20	25	50	40	0.981	1.489
301	20	25	50	40	1.962	1.208
302	20	25	50	40	2.943	1.001
303	20	25	50	40	3.924	0.842
304	20	30	20	30	0	1.056
305	20	30	20	30	0.981	0.851
306	20	30	20	35	0	1.275
307	20	30	20	35	0.981	1.027
308	20	30	20	35	1.962	0.843
309	20	30	20	40	0	1.522
310	20	30	20	40	0.981	1.225
311	20	30	20	40	1.962	1.006
312	20	30	20	40	2.943	0.838
313	20	30	30	30	0	1.067

(Continued)

Table A1 (continued)

S. No.	H/m	$\beta/°$	c/kPa	$\phi/°$	PGA/ms^{-2}	FoS
314	20	30	30	30	0.981	0.86
315	20	30	30	35	0	1.287
316	20	30	30	35	0.981	1.037
317	20	30	30	35	1.962	0.852
318	20	30	30	40	0	1.536
319	20	30	30	40	0.981	1.237
320	20	30	30	40	1.962	1.017
321	20	30	30	40	2.943	0.847
322	20	30	40	30	0	1.076
323	20	30	40	30	0.981	0.868
324	20	30	40	35	0	1.297
325	20	30	40	35	0.981	1.046
326	20	30	40	35	1.962	0.86
327	20	30	40	40	0	1.547
328	20	30	40	40	0.981	1.247
329	20	30	40	40	1.962	1.025
330	20	30	40	40	2.943	0.854
331	20	30	50	30	0	1.086
332	20	30	50	30	0.981	0.876
333	20	30	50	35	0	1.307
334	20	30	50	35	0.981	1.054
335	20	30	50	35	1.962	0.868
336	20	30	50	40	0	1.557
337	20	30	50	40	0.981	1.255
338	20	30	50	40	1.962	1.032
339	20	30	50	40	2.943	0.861
340	20	35	20	35	0	1.068
341	20	35	20	35	0.981	0.873
342	20	35	20	40	0	1.271
343	20	35	20	40	0.981	1.038
344	20	35	20	40	1.962	0.858
345	20	35	30	35	0	1.079
346	20	35	30	35	0.981	0.883
347	20	35	30	40	0	1.283
348	20	35	30	40	0.981	1.049
349	20	35	30	40	1.962	0.869
350	20	35	40	35	0	1.089
351	20	35	40	35	0.981	0.892
352	20	35	40	40	0	1.294
353	20	35	40	40	0.981	1.059
354	20	35	40	40	1.962	0.877

(Continued)

Table A1 (continued)

S. No.	H/m	$\beta/°$	c/kPa	$\phi/°$	PGA/ms^{-2}	FoS
355	20	35	50	35	0	1.1
356	20	35	50	35	0.981	0.902
357	20	35	50	40	0	1.305
358	20	35	50	40	0.981	1.068
359	20	35	50	40	1.962	0.887
360	25	20	20	20	0	1.037
361	25	20	20	20	0.981	0.784
362	25	20	20	25	0	1.322
363	25	20	20	25	0.981	1
364	25	20	20	25	1.962	0.793
365	25	20	20	30	0	1.633
366	25	20	20	30	0.981	1.235
367	25	20	20	30	1.962	0.979
368	25	20	20	35	0	1.975
369	25	20	20	35	0.981	1.494
370	25	20	20	35	1.962	1.184
371	25	20	20	35	2.943	0.968
372	25	20	20	40	0	2.362
373	25	20	20	40	0.981	1.786
374	25	20	20	40	1.962	1.416
375	25	20	20	40	2.943	1.157
376	25	20	20	40	3.924	0.966
377	25	20	30	20	0	1.046
378	25	20	30	20	0.981	0.791
379	25	20	30	25	0	1.342
380	25	20	30	25	0.981	1.008
381	25	20	30	25	1.962	0.799
382	25	20	30	30	0	1.643
383	25	20	30	30	0.981	1.243
384	25	20	30	30	1.962	0.985
385	25	20	30	35	0	1.986
386	25	20	30	35	0.981	1.502
387	25	20	30	35	1.962	1.191
388	25	20	30	35	2.943	0.973
389	25	20	30	40	0	2.374
390	25	20	30	40	0.981	1.795
391	25	20	30	40	1.962	1.423
392	25	20	30	40	2.943	1.163
393	25	20	30	40	3.924	0.972
394	25	20	40	20	0	1.053
395	25	20	40	20	0.981	0.797

(Continued)

Table A1 (continued)

S. No.	H/m	$\beta/°$	c/kPa	$\phi/°$	PGA/ms^{-2}	FoS
396	25	20	40	25	0	1.341
397	25	20	40	25	0.981	1.015
398	25	20	40	25	1.962	0.805
399	25	20	40	30	0	1.652
400	25	20	40	30	0.981	1.25
401	25	20	40	30	1.962	0.991
402	25	20	40	35	0	1.996
403	25	20	40	35	0.981	1.51
404	25	20	40	35	1.962	1.197
405	25	20	40	35	2.943	0.979
406	25	20	40	40	0	2.384
407	25	20	40	40	0.981	1.803
408	25	20	40	40	1.962	1.429
409	25	20	40	40	2.943	1.169
410	25	20	40	40	3.924	0.977
411	25	20	50	20	0	1.06
412	25	20	50	20	0.981	0.803
413	25	20	50	25	0	1.348
414	25	20	50	25	0.981	1.021
415	25	20	50	25	1.962	0.81
416	25	20	50	30	0	1.66
417	25	20	50	30	0.981	1.257
418	25	20	50	30	1.962	0.997
419	25	20	50	35	0	2.005
420	25	20	50	35	0.981	1.517
421	25	20	50	35	1.962	1.203
422	25	20	50	35	2.943	0.984
423	25	20	50	40	0	2.393
424	25	20	50	40	0.981	1.811
425	25	20	50	40	1.962	1.436
426	25	20	50	40	2.943	1.174
427	25	20	50	40	3.924	0.981
428	25	25	20	25	0	1.042
429	25	25	20	25	0.981	0.82
430	25	25	20	30	0	1.286
431	25	25	20	30	0.981	1.011
432	25	25	20	30	1.962	0.819
433	25	25	20	35	0	1.555
434	25	25	20	35	0.981	1.221
435	25	25	20	35	1.962	0.989
436	25	25	20	40	0	1.859

(Continued)

Table A1 (continued)

S. No.	H/m	$\beta/°$	c/kPa	$\phi/°$	PGA/ms^{-2}	FoS
437	25	25	20	40	0.981	1.46
438	25	25	20	40	1.962	1.182
439	25	25	20	40	2.943	0.978
440	25	25	30	25	0	1.052
441	25	25	30	25	0.981	0.827
442	25	25	30	30	0	1.296
443	25	25	30	30	0.981	1.019
444	25	25	30	30	1.962	0.826
445	25	25	30	35	0	1.565
446	25	25	30	35	0.981	1.231
447	25	25	30	35	1.962	0.997
448	25	25	30	40	0	1.87
449	25	25	30	40	0.981	1.47
450	25	25	30	40	1.962	1.191
451	25	25	30	40	2.943	0.985
452	25	25	40	25	0	1.06
453	25	25	40	25	0.981	0.834
454	25	25	40	30	0	1.305
455	25	25	40	30	0.981	1.026
456	25	25	40	30	1.962	0.832
457	25	25	40	35	0	1.575
458	25	25	40	35	0.981	1.238
459	25	25	40	35	1.962	1.004
460	25	25	40	35	2.943	0.831
461	25	25	40	40	0	1.88
462	25	25	40	40	0.981	1.478
463	25	25	40	40	1.962	1.198
464	25	25	40	40	2.943	0.992
465	25	25	50	25	0	1.067
466	25	25	50	25	0.981	0.84
467	25	25	50	30	0	1.313
468	25	25	50	30	0.981	1.033
469	25	25	50	30	1.962	0.838
470	25	25	50	35	0	1.583
471	25	25	50	35	0.981	1.246
472	25	25	50	35	1.962	1.01
473	25	25	50	35	2.943	0.837
474	25	25	50	40	0	1.889
475	25	25	50	40	0.981	1.486
476	25	25	50	40	1.962	1.204
477	25	25	50	40	2.943	0.997

(Continued)

Table A1 (continued)

S. No.	H/m	$\beta/°$	c/kPa	$\phi/°$	PGA/ms^{-2}	FoS
478	25	30	20	30	0	1.033
479	25	30	20	30	0.981	0.834
480	25	30	20	35	0	1.248
481	25	30	20	35	0.981	1.007
482	25	30	20	35	1.962	0.827
483	25	30	20	40	0	1.491
484	25	30	20	40	0.981	1.202
485	25	30	20	40	1.962	0.988
486	25	30	30	30	0	1.043
487	25	30	30	30	0.981	0.842
488	25	30	30	35	0	1.259
489	25	30	30	35	0.981	1.016
490	25	30	30	35	1.962	0.835
491	25	30	30	40	0	1.502
492	25	30	30	40	0.981	1.212
493	25	30	30	40	1.962	0.997
494	25	30	40	30	0	1.051
495	25	30	40	30	0.981	0.849
496	25	30	40	35	0	1.268
497	25	30	40	35	0.981	1.024
498	25	30	40	35	1.962	0.842
499	25	30	40	40	0	1.512
500	25	30	40	40	0.981	1.22
501	25	30	40	40	1.962	1.004
502	25	30	40	40	2.934	0.836
503	25	30	50	30	0	1.059
504	25	30	50	30	0.981	0.856
505	25	30	50	35	0	1.276
506	25	30	50	35	0.981	1.031
507	25	30	50	35	1.962	0.848
508	25	30	50	40	0	1.522
509	25	30	50	40	0.981	1.228
510	25	30	50	40	1.962	1.011
511	25	30	50	40	2.934	0.843
512	25	35	20	35	0	1.054
513	25	35	20	35	0.981	0.862
514	25	35	20	40	0	1.255
515	25	35	20	40	0.981	1.025
516	25	35	20	40	1.962	0.847
517	25	35	30	35	0	1.064
518	25	35	30	35	0.981	0.871

(Continued)

Table A1 (continued)

S. No.	H/m	$\beta/°$	c/kPa	$\phi/°$	PGA/ms^{-2}	FoS
519	25	35	30	40	0	1.266
520	25	35	30	40	0.981	1.035
521	25	35	30	40	1.962	0.856
522	25	35	40	35	0	1.074
523	25	35	40	35	0.981	0.879
524	25	35	40	40	0	1.276
525	25	35	40	40	0.981	1.044
526	25	35	40	40	1.962	0.864
527	25	35	50	35	0	1.082
528	25	35	50	35	0.981	0.887
529	25	35	50	40	0	1.285
530	25	35	50	40	0.981	1.052
531	25	35	50	40	1.962	0.871
532	30	20	20	20	0	1.036
533	30	20	20	20	0.981	0.783
534	30	20	20	25	0	1.322
535	30	20	20	25	0.981	0.999
536	30	20	20	30	0	1.632
537	30	20	20	30	0.981	1.234
538	30	20	20	30	1.962	0.977
539	30	20	20	35	0	1.975
540	30	20	20	35	0.981	1.493
541	30	20	20	35	1.962	1.182
542	30	20	20	35	2.934	0.966
543	30	20	20	40	0	2.363
544	30	20	20	40	0.981	1.786
545	30	20	20	40	1.962	1.414
546	30	20	20	40	2.943	1.155
547	30	20	20	40	3.924	0.965
548	30	20	30	20	0	1.043
549	30	20	30	20	0.981	0.789
550	30	20	30	25	0	1.33
551	30	20	30	25	0.981	1.006
552	30	20	30	25	1.962	0.797
553	30	20	30	30	0	1.641
554	30	20	30	30	0.981	1.241
555	30	20	30	30	1.962	0.983
556	30	20	30	35	0	1.985
557	30	20	30	35	0.981	1.501
558	30	20	30	35	1.962	1.189
559	30	20	30	35	2.943	0.972

(Continued)

Table A1 (continued)

S. No.	H/m	$\beta/°$	c/kPa	$\phi/°$	PGA/ms^{-2}	FoS
560	30	20	30	40	0	2.373
561	30	20	30	40	0.981	1.794
562	30	20	30	40	1.962	1.421
563	30	20	30	40	2.943	1.161
564	30	20	30	40	3.924	0.97
565	30	20	40	20	0	1.051
566	30	20	40	20	0.981	0.795
567	30	20	40	25	0	1.338
568	30	20	40	25	0.981	1.012
569	30	20	40	25	1.962	0.802
570	30	20	40	30	0	1.649
571	30	20	40	30	0.981	1.247
572	30	20	40	30	1.962	0.989
573	30	20	40	35	0	1.994
574	30	20	40	35	0.981	1.507
575	30	20	40	35	1.962	1.195
576	30	20	40	35	2.943	0.977
577	30	20	40	40	0	2.382
578	30	20	40	40	0.981	1.801
579	30	20	40	40	1.962	1.427
580	30	20	40	40	2.943	1.166
581	30	20	40	40	3.924	0.974
582	30	20	50	20	0	1.057
583	30	20	50	20	0.981	0.8
584	30	20	50	25	0	1.345
585	30	20	50	25	0.981	1.017
586	30	20	50	25	1.962	0.807
587	30	20	50	30	0	1.657
588	30	20	50	30	0.981	1.253
589	30	20	50	30	1.962	0.993
590	30	20	50	35	0	2.001
591	30	20	50	35	0.981	1.513
592	30	20	50	35	1.962	1.2
593	30	20	50	35	2.943	0.981
594	30	20	50	40	0	2.391
595	30	20	50	40	0.981	1.808
596	30	20	50	40	1.962	1.433
597	30	20	50	40	2.943	1.171
598	30	20	50	40	3.924	0.979
599	30	25	20	25	0	1.027
600	30	25	20	25	0.981	0.808

(Continued)

Table A1 (continued)

S. No.	H/m	$\beta/°$	c/kPa	$\phi/°$	PGA/ms^{-2}	FoS
601	30	25	20	30	0	1.266
602	30	25	20	30	0.981	0.997
603	30	25	20	35	0	1.532
604	30	25	20	35	0.981	1.206
605	30	25	20	35	1.962	0.977
606	30	25	20	40	0	1.831
607	30	25	20	40	0.981	1.441
608	30	25	20	40	1.962	1.168
609	30	25	20	40	2.943	0.966
610	30	25	30	25	0	1.035
611	30	25	30	25	0.981	0.815
612	30	25	30	30	0	1.275
613	30	25	30	30	0.981	1.004
614	30	25	30	30	1.962	0.815
615	30	25	30	35	0	1.541
616	30	25	30	35	0.981	1.213
617	30	25	30	35	1.962	0.984
618	30	25	30	40	0	1.841
619	30	25	30	40	0.981	1.45
620	30	25	30	40	1.962	1.175
621	30	25	30	40	2.943	0.973
622	30	25	40	25	0	1.042
623	30	25	40	25	0.981	0.821
624	30	25	40	30	0	1.283
625	30	25	40	30	0.981	1.011
626	30	25	40	30	1.962	0.82
627	30	25	40	35	0	1.55
628	30	25	40	35	0.981	1.221
629	30	25	40	35	1.962	0.99
630	30	25	40	40	0	1.851
631	30	25	40	40	0.981	1.457
632	30	25	40	40	1.962	1.182
633	30	25	40	40	2.943	0.978
634	30	25	50	25	0	1.048
635	30	25	50	25	0.981	0.826
636	30	25	50	30	0	1.29
637	30	25	50	30	0.981	1.017
638	30	25	50	30	1.962	0.825
639	30	25	50	35	0	1.557
640	30	25	50	35	0.981	1.227
641	30	25	50	35	1.962	0.996

(Continued)

Table A1 (continued)

S. No.	H/m	$\beta/°$	c/kPa	$\phi/°$	PGA/ms^{-2}	FoS
642	30	25	50	40	0	1.859
643	30	25	50	40	0.981	1.464
644	30	25	50	40	1.962	1.188
645	30	25	50	40	2.943	0.983
646	30	30	20	30	0	1.037
647	30	30	20	30	0.981	0.835
648	30	30	20	35	0	1.253
649	30	30	20	35	0.981	1.01
650	30	30	20	35	1.962	0.829
651	30	30	20	40	0	1.497
652	30	30	20	40	0.981	1.206
653	30	30	20	40	1.962	0.99
654	30	30	30	30	0	1.046
655	30	30	30	30	0.981	0.843
656	30	30	30	35	0	1.262
657	30	30	30	35	0.981	1.018
658	30	30	30	35	1.962	0.836
659	30	30	30	40	0	1.507
660	30	30	30	40	0.981	1.215
661	30	30	30	40	1.962	0.998
662	30	30	40	30	0	1.053
663	30	30	40	30	0.981	0.849
664	30	30	40	35	0	1.271
665	30	30	40	35	0.981	1.025
666	30	30	40	35	1.962	0.843
667	30	30	40	40	0	1.517
668	30	30	40	40	0.981	1.223
669	30	30	40	40	1.962	1.005
670	30	30	40	40	2.943	0.837
671	30	30	50	30	0	1.06
672	30	30	50	30	0.981	0.856
673	30	30	50	35	0	1.278
674	30	30	50	35	0.981	1.031
675	30	30	50	35	1.962	0.848
676	30	30	50	40	0	1.524
677	30	30	50	40	0.981	1.229
678	30	30	50	40	1.962	1.011
679	30	30	50	40	2.943	0.843
680	30	35	20	35	0	1.045
681	30	35	20	35	0.981	0.855
682	30	35	20	40	0	1.245

(Continued)

Table A1 (continued)

S. No.	H/m	$\beta/°$	c/kPa	$\phi/°$	PGA/ms^{-2}	FoS
683	30	35	20	40	0.981	1.017
684	30	35	20	40	1.962	0.84
685	30	35	30	35	0	1.055
686	30	35	30	35	0.981	0.863
687	30	35	30	40	0	1.255
688	30	35	30	40	0.981	1.026
689	30	35	30	40	1.962	0.848
690	30	35	40	35	0	1.063
691	30	35	40	35	0.981	0.87
692	30	35	40	40	0	1.264
693	30	35	40	40	0.981	1.034
694	30	35	40	40	1.962	0.855
695	30	35	50	35	0	1.07
696	30	35	50	35	0.981	0.877
697	30	35	50	40	0	1.272
698	30	35	50	40	0.981	1.041
699	30	35	50	40	1.962	0.861
700	30	35	50	40	1.962	0.861